

Coherent imaging at resolution beyond diffraction limit using post-experimental data extrapolation

Tatiana Latychevskaia & Hans-Werner Fink

Physics Institute, University of Zurich,

Winterthurerstrasse 190, CH- 8057 Zürich, Switzerland

Classical microscopy, regardless if photons or electrons are used, is based on incoherent optics and the microscopic record represents a distribution of added intensities. Local information of the sample is thus mapped onto local information at the detector. The resultant image exhibits a resolution ultimately limited by the Abbe criterion¹ respectively by the numerical aperture of the microscope for a given wavelength. A number of super-resolution techniques in near²⁻³ as well as in the far-field⁴⁻⁸ have been proposed which allow imaging beyond the Abbe resolution limit. In contrast to classical optical microscopy in coherent microscopy, like holography⁹⁻¹⁰ or coherent diffraction¹¹, the superposition principle of waves holds, implying that field amplitudes are added, not intensities. The superposition of waves, be it light or deBroglie waves, leads to a non-local representation of the microscopic object information, an interference pattern spread out in space beyond the scattering object. Here we show a novel super-resolution technique based on the fact that this interference information combined with the wave continuity allows wave extrapolation beyond the detected area and thus circumventing the resolution limit imposed by the Abbe criterion. It is a generally accepted notion that once a microscopy experiment has been carried out, the resolution of the experimental record is an intrinsic property of the various experimental parameters and thus fixed once the experiment has been completed. We show that this notion is not valid when

coherent radiation is used. In fact, fine details, originally not available in the actual experimental record can retrospectively be recovered from just a fraction of an interference pattern. Our technique can be applied to images obtained by any coherent imaging technique, and by any coherent type of radiation, be it light, X-rays or electrons.

Ever since Ernst Karl Abbe introduced the term “Numerical Aperture” (N.A.) and proposed the resolution criterion $R=\lambda/(2N.A.)$, it has been the quantitative measure of optical system performance until today. However, with the invention of optical lasers, and later, coherent X-ray and electron sources, imaging techniques employing coherent waves have been developed, and here the Abbe’s criterion is only remotely related to the possibly achievable resolution. Coherent radiation, despite of many obvious advantages, deteriorates the resolution due to interference effects between the scattered waves. For example, for two point scatterers, the total intensity in case of incoherent radiation is given by: $I = |U_1|^2 + |U_2|^2$ where U_1 and U_2 are complex-valued waves diffracted by scatterers 1 and 2 while in case of coherent radiation, the total intensity is given by $I = |U_1|^2 + |U_2|^2 + U_1 U_2^* + U_1^* U_2$. Now, the interference term $U_1 U_2^* + U_1^* U_2$ “blurs” the image of two scatterers. However, this very interference term contains the phase information about the interfering waves, and, in the technique we propose here, it allows reconstructing the entire complex-valued wavefront created by the scatterers.

In a typical experiment, a finite fraction of an interference pattern I_0 , such as a hologram or coherent diffraction pattern, is recorded by a detector of size $S_0 \times S_0$, and digitized with $N_0 \times N_0$ pixels, so that $S_0 = N_0 \Delta$, where Δ is the pixel size of the detector. The complex-valued wave U_0 forming the interference pattern I_0 can be reconstructed by employing conventional numerical methods. The back-propagation of the wave U_0 to the object domain results in the

reconstruction of the object at a resolution provided by the Abbe criterion $R_0=\lambda/(2N.A_0)$, where $N.A_0$ is limited by the detector size S_0 . However, the distribution U_0 is complex-valued and thus contains sufficient information to uniquely define the elementary waves scattered by the object. These elementary waves can be extrapolated beyond the original interference pattern I_0 , and thus effectively increase the numerical aperture and hence the resolution. For extrapolation, an iterative routine is applied, which boils down to the wavefront propagation between detector and object plane, see Supplementary Information and Fig. S1. For the first iteration, the reconstructed complex-valued distribution U_0 of the size $\Delta N_0 \times \Delta N_0$ (or $S_0 \times S_0$) is extended onto an area $\Delta N \times \Delta N$ (or $S \times S$) by padding U_0 with random complex-valued numbers. Here $N > N_0$ (or $S > S_0$) while the pixel size Δ remains unchanged. The random numbers are updated after each iteration and eventually turn into an extrapolated interference pattern beyond the experimental record. In the object plane, we assume the object to have a finite size and it is masked by a limiting support. Additional constraints, such as a real, positive and finite transmission function of the object, can also be applied¹². The resulting self-extrapolated interference pattern of size $S \times S$ provides a nominally larger numerical aperture $N.A. > N.A_0$. As a consequence, a resolution better than R_0 , respectively beyond the diffraction limit is achieved in the reconstructed object.

To demonstrate our method we select the most popular modern coherent imaging techniques - coherent diffraction imaging (CDI)¹¹. CDI allows a complete recovery of a non-periodic object from its far-field diffraction pattern, provided the latter is sampled with at least twice the Nyquist frequency (oversampling)¹³, by using one of the iterative phase retrieval routines¹⁴⁻¹⁷. These routines are based on back and forward propagation of the optical field between detector and object plane, calculated by Fourier transforms. Since numerical Fourier-transformations are performed on finite sized images, this imposes another default constraint: the experimental diffraction pattern is surrounded by zeros, while in an idealized

experiment it is not. The experimentally recorded diffraction pattern can thus be regarded as a cropped version of a diffraction pattern spread out over an extended range in space. Mathematically, this can be represented as a product of a true infinite diffraction pattern with a two-dimensional screen aperture. As a result, the object reconstruction is always blurred by the convolution with a two-dimensional far-field distribution of the screen aperture.

By applying our technique we just remove the constraint of the diffraction pattern being zero-padded and instead let the experimental diffraction pattern extrapolate itself. As a result, the reconstructed object, being the spectrum of the self-extrapolated interference pattern, is better resolved than the reconstructed object from the non-extrapolated interference pattern, see Supplementary Information and Fig. S2.

A simulated interference pattern created by two coherent point sources is shown in Fig. 1. The intensity distribution in the far-field resembles an equidistant fringes pattern. When this far-field diffraction pattern is recorded in the oversampling regime, the two scatterers can be recovered by using one of the iterative phase retrieval methods¹⁴. When just a fraction of the interference pattern I_0 (of size 200×200 pixels) is available, as shown in Fig.1a, the related complex-valued wave distribution at the detector U_0 is retrieved (see Supplementary Information for details), but the two reconstructed point sources are barely resolved, see Fig. 1b. Here, the poor resolution of the reconstruction is given by the limited extend of the diffraction pattern I_0 . Next, we extrapolate the recovered U_0 as described above. In the first iteration we pad the outside region of U_0 up to 1000×1000 pixels with random numbers and allow for updating the values of these pixels after each iterative run. After 2000 iterations, the interference pattern extrapolated itself beyond the area of the actual data of I_0 (marked with a red square), see Fig. 1c. As a result, the N.A. has effectively been increased and the reconstruction of the self-extrapolated diffraction pattern demonstrates superior resolution; the two point sources are now clearly resolved, as shown in Fig. 1d. Thus, from just a fraction

of a diffraction pattern it is possible to extrapolate the interference pattern beyond the recorded area and, eventually, enhance the resolution.

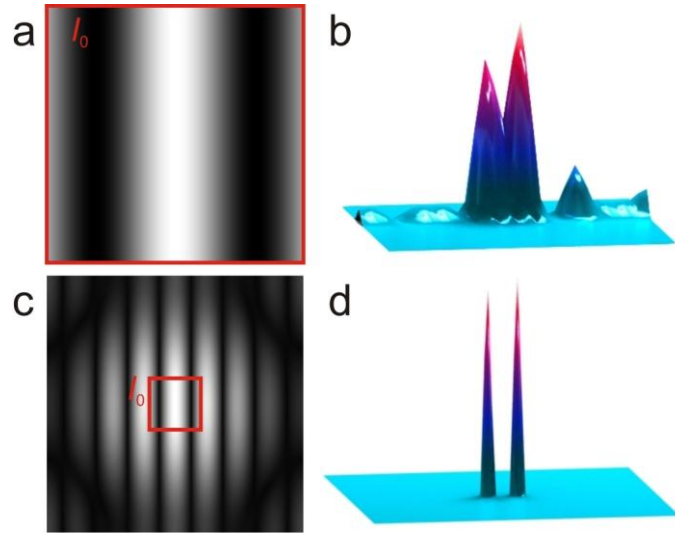


Figure 1. Self-extrapolated interference pattern of two point sources. **a**, I_0 , a 200×200 pixels fragment of the amplitude of the interference pattern created by two coherent point sources. **b**, Reconstruction from the interference pattern shown in (a) obtained after 300 iterations using hybrid input output algorithm (HIO). The two point sources are barely resolved. **c**, Self-extrapolated up to 1000×1000 pixels interference pattern after 2000 iterations. **d**, Reconstruction of the self-extrapolated interference pattern shown in (c). The two point sources are clearly resolved.

When it comes to experimental data the challenge is to correctly sample the waves constituting the interference pattern. Next to the well-known Shannon-Nyquist sampling criterion¹⁸⁻²⁰, an accurate sampling of the *intensities* must also be fulfilled (see Supplementary Information and Fig. S3). Therefore, it is essential to sample the interference pattern with a high dynamic range in the intensities. However, even a conventional CCD

camera with a 10 bit dynamic range, as used for our experimental data, is sufficient to fulfil this requirement.

Optical diffraction patterns were recorded using 532 nm wavelength laser light. As sample we used a microscope cover slip on which a thin layer of gold was evaporated. A focussed ion beam was used to engrave a pattern displaying a “Ψ”, a “2” and four circles, as shown in Fig. 2a. The diffraction pattern of this sample, recorded with an oversampling ratio of 9 in both dimensions, is shown in Fig. 2b, and its reconstruction in Fig. 2c. The intrinsic resolution of the recorded diffraction pattern²¹, according to the Abbe criterion, amounts to 1.8 μm , being in good agreement with the quality of the reconstruction. Next, we crop the diffraction pattern keeping only its central 300×300 pixels part I_0 , as depicted in Fig. 2d. The intrinsic resolution of the cropped diffraction pattern I_0 amounts to only 5.9 μm . As a consequence, its reconstruction resembles a blurred object, shown in Fig. 2e. Next, we apply our extrapolation technique to recreate the high-resolution information from the cropped diffraction pattern I_0 . The complex-valued field distribution U_0 at the detector is padded up to 1000×1000 pixels with random values and reconstructed with the same algorithm as already described above. After 1000 iterations the diffraction pattern has extrapolated itself beyond I_0 as shown in Fig. 2f. Due to this effectively increased N.A, the reconstruction of the self-extrapolated diffraction pattern, shown in Fig. 2g, exhibits an enhanced resolution compared to (e), fine fringes are now apparent and well resolved. The post-experimental treatment of the detected wave field thus allows circumventing the resolution limit imposed by the Abbe criterion.

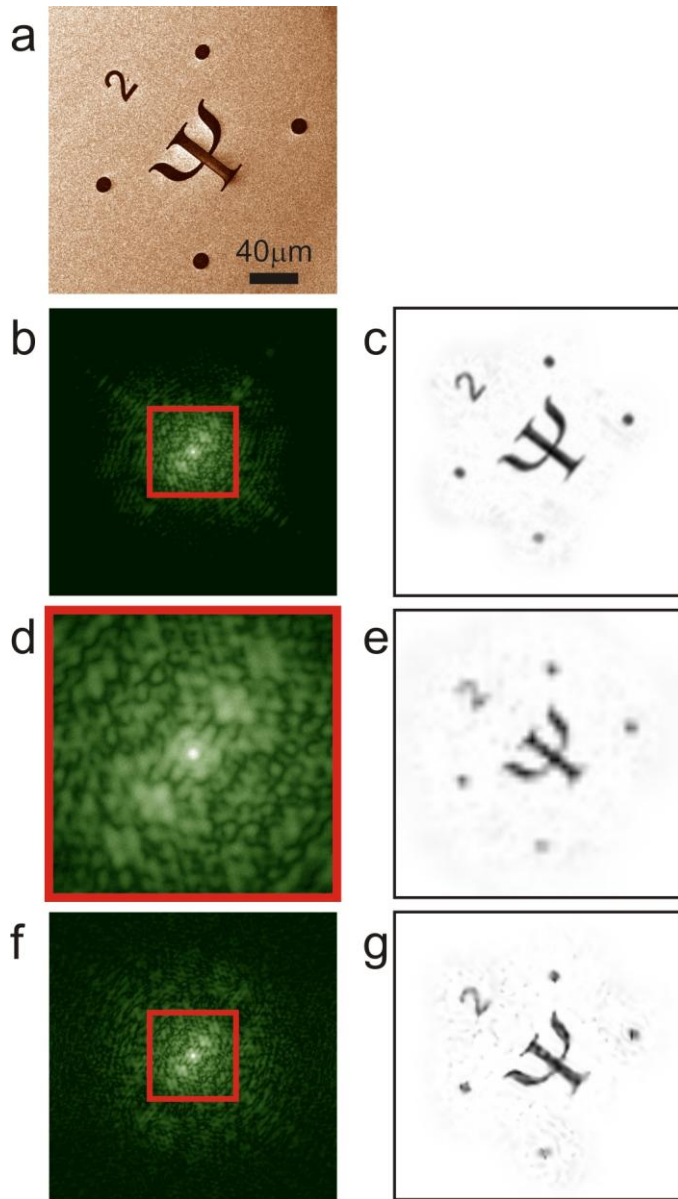


Figure 2. Self-extrapolated experimental diffraction pattern. **a**, Scanning electron microscope image of the sample. **b**, Amplitude of the optical diffraction pattern, recorded at 60 cm distance from the sample with 532 nm wavelength laser light. The diffraction pattern was imaged at a screen of size $181 \times 181 \text{ mm}^2$ and sampled with 1000×1000 pixels using 10 bit camera. To capture the intensity variations in the central part and at the rim of the diffraction pattern, a set of images was recorded at various exposures and those were combined into a high dynamic range diffraction pattern. **c**, Its reconstruction. After 64 iteration using hybrid input output (HIO) algorithm with the feedback parameter $\beta = 0.9$ and

*a loose mask support in the object domain, the mask was updated to more tight one and additional 1000 iterations using error-reduction (ER) algorithm were performed. **d**, A 300×300 pixels fragment of the amplitude of the experimental diffraction I_0 , indicated with red square. **e**, Reconstruction of the fragment of the diffraction pattern I_0 obtained after 100 iterations using HIO algorithm with a loose object mask followed by 400 iterations using error-reduction (ER) algorithm with a tight object mask. **f**, Amplitude of the self-extrapolated up to 1000×1000 pixels diffraction pattern after total 1000 iterations using ER algorithm. **g**, Reconstruction of the self-extrapolated diffraction pattern shown in (f). Amplitude of the diffraction pattern in (b), (d) and (f) is shown in logarithmic scale.*

To cross-validate our method, we also performed the same iterative reconstruction procedure but with zero padding during the entire retrieval routine. The result shows just a blurred reconstruction of the original object, see Supplementary Fig. S4.

Our new scheme of self-extrapolation is applicable to any interference patterns created by elastic scattering from a non-periodic object. A limited size low-resolution interference pattern is sufficient to recreate a high-resolution reconstruction of the object. This implies that, even without any additional experiments, the resolution in previously reconstructed experimental data can be enhanced by applying our technique. While our technique can be applied to any kind of radiation, be it be X-rays, photons or electrons, the following conditions must be fulfilled: (1) A sufficiently coherent source must be used in order to provide an interference pattern with good contrast. (2) The detector should be capable to capture the interference pattern with a high dynamic intensity range. (3) The scattering object must be of finite size. Although we related this novel tool to diffraction patterns here, the method can be applied to any other interference patterns, for instance, created by Fresnel coherent diffraction imaging²², Fourier-transform²³ or classical Gabor type holography^{9-10,24}.

Acknowledgements

We would like to thank Michael Krueger for the sample preparation. The work presented here is financially supported by the Swiss National Science Foundation (SNF).

Author contributions

T.L. had the idea for this technique, made the simulations, designed and conducted the experiment. T. L. and H.-W. F. worked together to interpret the results and to write the manuscript.

References

- 1 Abbe, E. The realtion of aperture and power in the microscope. *Journal of the Royal Microscopical Society* **2**, 300-309 (1883).
- 2 Pohl, D. W., Denk, W. & Lanz, M. Optical stethoscopy - image recording with resolution $\lambda/20$. *Appl. Phys. Lett.* **44**, 651-653 (1984).
- 3 Schuck, P. J., Fromm, D. P., Sundaramurthy, A., Kino, G. S. & Moerner, W. E. Improving the mismatch between light and nanoscale objects with gold bowtie nanoantennas. *Phys. Rev. Lett.* **94**, 017402 (2005).
- 4 Hell, S. W., Stelzer, E. H. K., Lindek, S. & Cremer, C. Confocal microscopy with an increased detection aperture - type B 4 pi confocal microscopy. *Opt. Lett.* **19**, 222-224 (1994).
- 5 Hell, S. W. & Wichmann, J. Breaking the diffraction resolution limit by stimulated emission - stimulated emission depletion fluorescence microscopy. *Opt. Lett.* **19**, 780-782 (1994).
- 6 Gustafsson, M. G. L. Surpassing the lateral resolution limit by a factor of two using structured illumination microscopy. *J. Microsc.-Oxf.* **198**, 82-87 (2000).
- 7 Betzig, E. *et al.* Imaging intracellular fluorescent proteins at nanometer resolution. *Science* **313**, 1642-1645 (2006).
- 8 Huang, B., Wang, W. Q., Bates, M. & Zhuang, X. W. Three-dimensional super-resolution imaging by stochastic optical reconstruction microscopy. *Science* **319**, 810-813 (2008).
- 9 Gabor, D. A new microscopic principle. *Nature* **161**, 777-778 (1948).
- 10 Gabor, D. Microscopy by reconstructed wave-fronts. *Proc. R. Soc. A* **197**, 454-487 (1949).
- 11 Miao, J. W., Charalambous, P., Kirz, J. & Sayre, D. Extending the methodology of x-ray crystallography to allow imaging of micrometre-sized non-crystalline specimens. *Nature* **400**, 342-344 (1999).
- 12 Latychevskaia, T. & Fink, H.-W. Solution to the twin image problem in holography. *Phys. Rev. Lett.* **98**, 233901 (2007).
- 13 Sayre, D. Some implications of a theorem due to Shannon. *Acta Crystallogr.* **5**, 843-843 (1952).
- 14 Fienup, J. R. Phase retrieval algorithms - a comparison. *Appl. Optics* **21**, 2758-2769 (1982).

15 Marchesini, S. *et al.* X-ray image reconstruction from a diffraction pattern alone. *Phys. Rev. B* **68** (2003).

16 Latychevskaia, T., Longchamp, J.-N. & Fink, H.-W. Novel Fourier-domain constraint for fast phase retrieval in coherent diffraction imaging. *Opt. Express* **19**, 19330-19339 (2011).

17 Fienup, J. R. Phase retrieval algorithms: a personal tour. *Appl. Optics* **52**, 45-56 (2013).

18 Nyquist, H. Certain topics in telegraph transmission theory. *Trans. AIEE* **47**, 617–644 (1928).

19 Kotelnikov, V. A. On the transmission capacity of "ether" and wire in electrocommunications. *Izd. Red. Upr. Svyazi RKKA* (1933).

20 Shannon, C. E. Communication in the presence of noise. *Proc. IEEE* **86**, 447-457 (1949).

21 Latychevskaia, T., Longchamp, J.-N. & Fink, H.-W. When holography meets coherent diffraction imaging *Opt. Express* **20**, 28871-28892 (2012).

22 Williams, G. J. *et al.* Fresnel coherent diffractive imaging. *Phys. Rev. Lett.* **97**, 025506 (2006).

23 Stroke, G. W. Lensless Fourier-transform method for optical holography *Appl. Phys. Lett.* **6**, 201-& (1965).

24 Latychevskaia, T. & Fink, H.-W. Resolution enhancement in digital holography by self-extrapolation of holograms. *Opt. Express* **21**, 7726-7733 (2013).

Supplementary information

The iterative extrapolation routine

The procedure for iterative extrapolation is illustrated in Fig. S1 and includes the following steps:

- (i) Formation of the input of the complex-valued field in the detector plane $U(x_s, y_s)$. The amplitude of the central $S_0 \times S_0$ part (sampled with $N_0 \times N_0$ pixels) is replaced by the square root of the measured intensity $|U_0(x_s, y_s)|$ after each iteration. The amplitude of the remaining $S \times S$ part (sampled with $N \times N$ pixels) is randomly distributed at the first iteration and updated after each iteration. The phase distribution after the first iteration is composed of the phase distribution of $U_0(x_s, y_s)$ for the central $S_0 \times S_0$ part and a random distribution with numbers in the range $[-\pi, \pi]$ fills up the remaining pixels of the extended $S \times S$ matrix. The entire phase distribution is updated after each iteration.
- (ii) Back propagation to the object plane. In the case of coherent diffraction imaging, it is calculated by a backward Fourier transform. In the case of holography, the integral transformation given by the Fresnel-Huygens principle must be computed²⁵.
- (iii) In the object plane, the following constraints are applied to the reconstructed complex-valued object distribution $o(x_o, y_o)$. Since the object exhibits a finite size, the distribution $o(x_o, y_o)$ is multiplied with a loose mask which sets the values outside the mask to zero²⁶, see Fig. S1. A second constraint is that of positive absorption¹² demanding that the pixel values where absorption is negative are set to zero. This results in an updated transmission function $o'(x_o, y_o)$.
- (iv) The updated complex-valued wavefront in the screen plane $U'(x_s, y_s)$ is obtained by forward propagation and its amplitude and phase distributions are the input values for the next iteration starting at step (i).

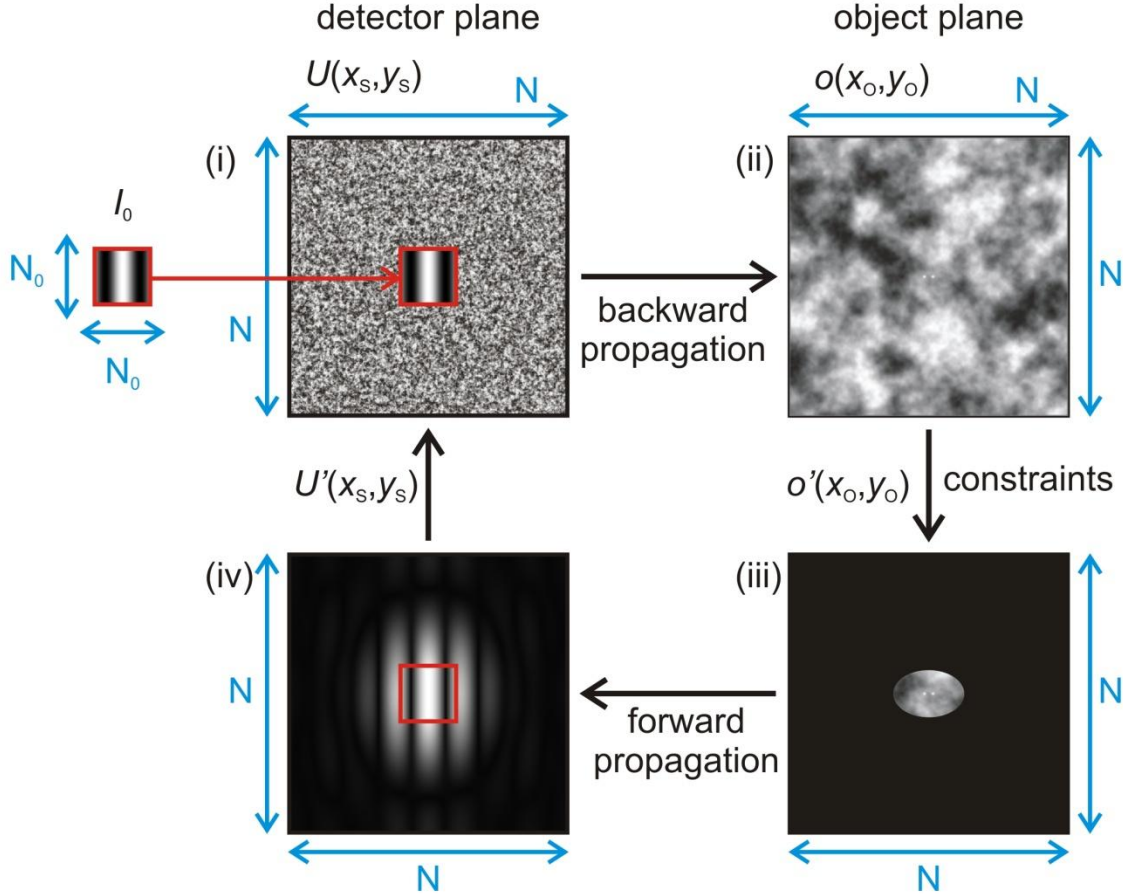


Figure S1: Flow diagram of the iterative reconstruction scheme.

Size of the interference pattern and related spatial resolution

Here we demonstrate how the resolution of the reconstructed object depends on the size of the detector, provided the pixel size of the detector remains unchanged. An interference pattern is created by two coherent waves of wavelength $\lambda = 500$ nm and amplitude A originating from two sources that are $d = 10$ μm spaced apart:

$$U(\theta) = 2A \cos\left(\frac{2\pi}{\lambda} d \sin \theta\right). \quad (\text{S1})$$

The intensity profile of the interference pattern as a function of the diffraction angle θ is shown in Fig. S2, where we assumed $A = 1$. When the detected part of the interference pattern is limited by $\theta = [-0.05\pi, 0.05\pi]$ and sampled with 200 points, as shown in Fig. S2a, its spectrum shows two distinct peaks that correspond to the two point sources, see Fig. S2b.

When only half of the same intensity distribution is detected with $\theta = [-0.025\pi, 0.025\pi]$ and sampled with the same the sampling rate (thus over 100 points), see Fig. S2c, the peaks in the resultant spectrum get broadened and overlap, as shown in Fig. S2d.

By extrapolating the signal over a larger area, we do not add new information since the spectrum (the two point sources) remains the same. However, we do uncover the “hidden” spectral information by better resolving the spectrum. Digital Fourier transform implies that the bin size in the spectrum (object) domain is given by $1/S$, where S is the size of the area where the interference signal is available. Thus, when the signal is just extrapolated on a larger area S , the bin size given by $1/S$ becomes smaller, and the spectrum is better resolved.

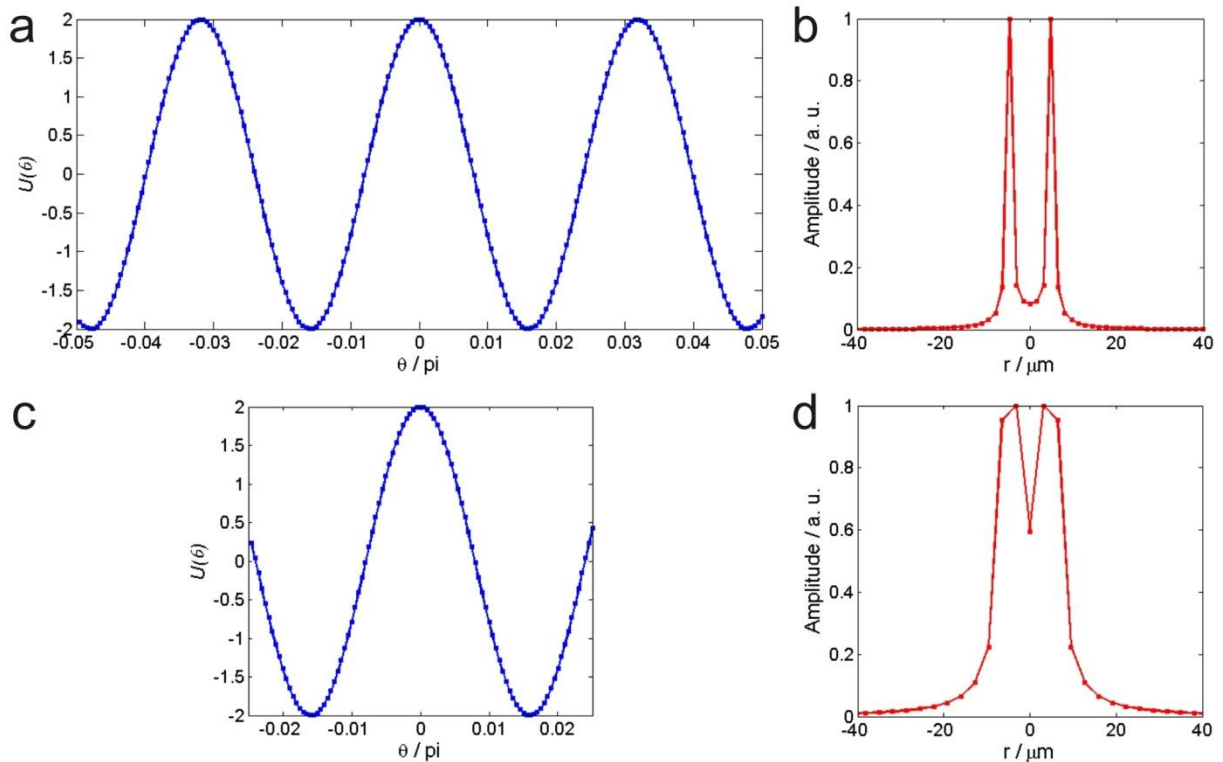


*Figure S2: Interference pattern created by two coherent sources as a function of diffraction angle θ and its spectrum. **a**, Profile of the interference pattern sampled at 200 points in the range $\theta = [-0.05\pi, 0.05\pi]$. **b**, Amplitude of the spectrum of (a). **c**, Profile of the interference pattern sampled with 100 points in the range $\theta = [-0.025\pi, 0.025\pi]$. **d**, Amplitude of the spectrum of (c).*

Simulated example

The amplitude of the far-field intensity distribution created by two closely spaced sources was simulated as the amplitude of a Fourier transform of a matrix of 1000×1000 pixels with zeros, whereby only two pixels in the centre, at a distance of 8 pixels from each other, are set to 1. I_0 is a small part of 200×200 pixels cut out from the simulated far-field amplitude distribution, as shown in Fig. 1a. The complex-valued wave U_0 was reconstructed from I_0 using 300 iterations using the hybrid input output (HIO) algorithm¹⁴ with a feedback parameter $\beta = 0.9$, positive absorption constraint¹² and a round mask of 30 pixels in diameter in the object domain; the result of the reconstruction is shown in Fig. 1b. The resultant U_0 was then extrapolated in the following manner. It was first padded up to 1000×1000 pixels with complex-valued random numbers of amplitudes in the range $[0,2]$ and phases in the range $[-\pi, \pi]$, and further reconstructed using the error-reduction algorithm¹⁴. In the iterative procedure the following constraint was applied in the detector plane: the amplitudes of the central 200×200 pixels were replaced with the square root of I_0 , and the amplitudes of the remaining pixels as well the phases of all pixels were updated after each iteration. In the object domain, the constraint of positive absorption¹² was applied. For the first 100 iterations, the object was confined within a limited region in space by setting the values outside an elliptical mask (with 100 pixels major and 60 pixels minor axis) to zero. Thereafter, the elliptical mask was tightened (with 23 pixels major and 13 pixels minor axis). A total of 2000 iterations were performed.

Resolution limitation in the extrapolation method

An individual scatterer is resolvable in the object domain when the corresponding diffracted wave is distinguishable in the recorded diffraction pattern. Therefore, the challenge here is

the correct sampling of the *dynamics of the intensity* of the diffraction pattern, as illustrated in Fig. S3. The object is selected in the form of the word “resolution” and the point in the letter “i” mimics the point-like scatterer. The object is sufficiently zero-padded to provide a high oversampling ratio. The size of the object area is $1 \times 1 \text{ mm}^2$, and it is sampled with 1000×1000 pixels. The point-like scatterer occupies a size of only 1×1 pixel, *i.e.* $1 \times 1 \text{ } \mu\text{m}^2$, see Fig. S3a. The two diffraction patterns, that of the one with and the one without the point-like scatterer, are simulated at a distance of 1 m from the sample using a wavelength of 500 nm and sampled with 1000×1000 pixels, see Fig. S3b and Fig. S3d. Both diffraction patterns show a resolution of $1 \text{ } \mu\text{m}$.

These two diffraction patterns seem identical at a first glance. The wave scattered by the point-like scatterer is spread out over the intensity distribution shown in Fig. S3b and its presence can only be detected by looking at the difference between the two intensities distributions. To mimic experimental conditions, the intensity distributions are sampled with a dynamic intensity range provided by modern digital detectors: 20 bits (1048576 bins) and 16 bits (65536 bins). The profiles of the intensity difference along the blue lines in the diffraction patterns Fig. S3b,d are shown in Fig. S3e. Two conclusions can be drawn from the results shown in Fig. S3e: (1) Although, the central 500×500 pixels part of the diffraction pattern provides only low-resolution information up to $2 \text{ } \mu\text{m}$, it already contains signal originated from the point-like scatterer of size $1 \times 1 \text{ } \mu\text{m}^2$, that is, it contains high-resolution information. (2) The better the dynamic range in the detected intensity the better the ability to detect signal from the point-like scatterer. Note the different amplitude range in Fig. S3e for 20 respectively 16 bits.

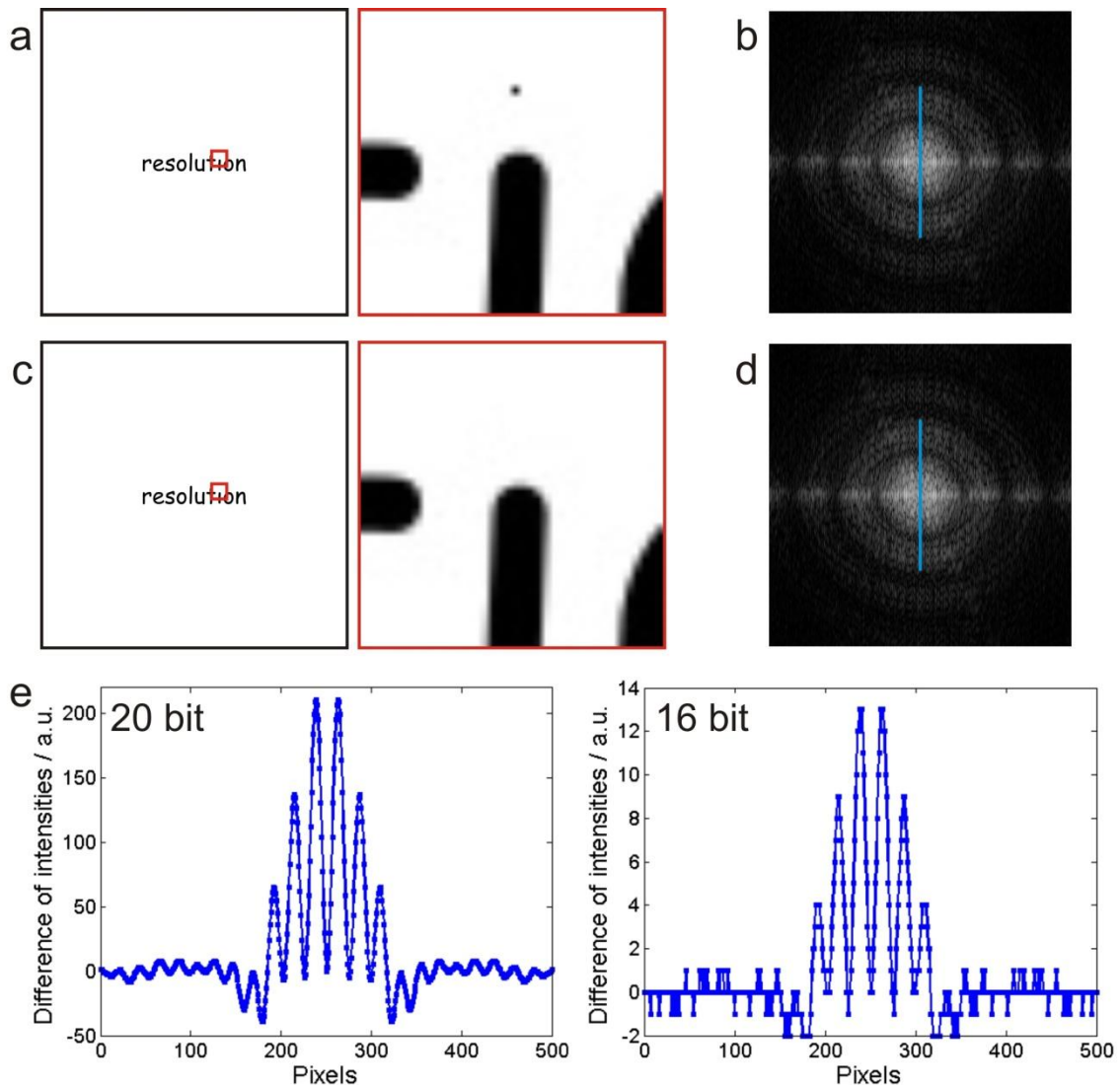


*Figure S3: Diffraction patterns with and without a point-like scatterer and their intensity sampling. **a**, Object in form of the word “resolution” with the point scatterer in the letter “i”, see the magnified inset in the red square. **b**, Simulated diffraction pattern of (a) shown in logarithmic scale. **c**, Object in form of the word “resolution” without the point scatterer in the letter “i”, see magnified inset in the red square. **d**, Simulated diffraction pattern of (c) shown in logarithmic scale. **e**, Difference between the intensities along the blue lines in (b) and (d) when the intensity is sampled with 20 respectively only 16 bit.*

Experimental example

To check that the resolution enhancement is not just due to the padding of the diffraction pattern and/or the iterative procedure, we set all the padded pixel values to zero during the entire retrieval routine. The reconstruction procedure was identical to the one for the other experimental diffraction patterns, using ER algorithm with positive absorption constraint and support mask in the object domain. The reconstruction obtained after 1000 iterations shows a blurred image of the original object, see Fig. S4.

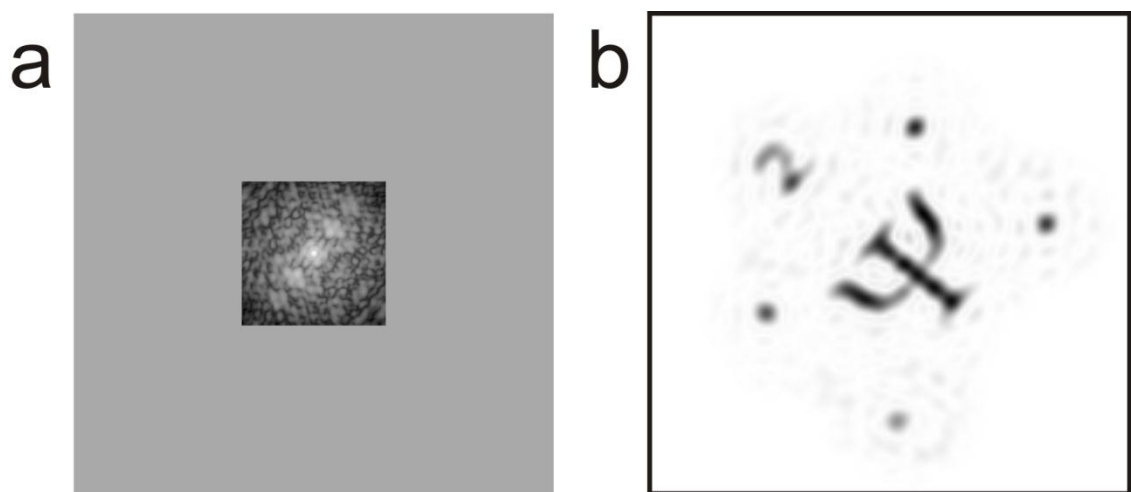


Figure S4: Reconstruction of zero-padded experimental diffraction pattern. a, Amplitude of the zero-padded diffraction pattern. b, Its reconstruction achieved after 1000 iterations using HIO algorithm.

References to Supplementary information

- 1 Latychevskaia, T. & Fink, H.-W. Simultaneous reconstruction of phase and amplitude contrast from a single holographic record. *Opt. Express* **17**, 10697-10705 (2009).
- 2 Latychevskaia, T., Formanek, P., Koch, C. T. & Lubk, A. Off-axis and inline electron holography: Experimental comparison. *Ultramicroscopy* **110**, 472-482 (2010).
- 3 Latychevskaia, T. & Fink, H.-W. Solution to the twin image problem in holography. *Phys. Rev. Lett.* **98**, 233901 (2007).
- 4 Fienup, J. R. Phase retrieval algorithms - a comparison. *Appl. Optics* **21**, 2758-2769 (1982).